Experimental investigation of defect-assisted and intrinsic water vapor permeation through ultrabarrier films

Hyungchul Kim, Ankit Kumar Singh, Cheng-Yin Wang, Canek Fuentes-Hernandez, Bernard Kippelen, and Samuel Graham

Citation: Review of Scientific Instruments **87**, 033902 (2016); doi: 10.1063/1.4942510
View online: https://doi.org/10.1063/1.4942510
View Table of Contents: http://aip.scitation.org/toc/rsi/87/3
Published by the American Institute of Physics

Experimental investigation of defect-assisted and intrinsic water vapor permeation through ultrabarrier films

Hyungchul Kim,[1] Ankit Kumar Singh,[2] Cheng-Yin Wang,[3] Canek Fuentes-Hernandez,[3] Bernard Kippelen,[3] and Samuel Graham[1,2]
[1]*Woodruff School of Mechanical Engineering, Georgia Institute of Technology, Atlanta, Georgia 30332, USA*
[2]*School of Materials Science and Engineering, Georgia Institute of Technology, Atlanta, Georgia 30332, USA*
[3]*School of Electrical and Computer Engineering, and Center for Organic Photonics and Electronics, Georgia Institute of Technology, Atlanta, Georgia 30332, USA*

(Received 25 August 2015; accepted 23 January 2016; published online 15 March 2016)

In the development of ultrabarrier films for packaging electronics, the effective water vapor transmission rate is a combination of permeation through pinhole defects and the intrinsic permeation through the actual barrier film. While it is possible to measure the effective permeation rate through barriers, it is important to develop a better understanding of the contribution from defects to the overall effective barrier performance. Here, we demonstrate a method to investigate independently defect-assisted permeation and intrinsic permeation rates by observing the degradation of a calcium layer encapsulated with a hybrid barrier film, that is, prepared using atomic layer deposition (ALD) and plasma enhanced deposition (PECVD). The results are rationalized using an analytical diffusion model to calculate the permeation rate as a function of spatial position within the barrier. It was observed that a barrier film consisting of a PECVD SiN_x layer combined with an ALD Al_2O_3/HfO_x nanolaminate resulted in a defect-assisted water vapor transmission rate (WVTR) of 4.84×10^{-5} g/m^2 day and intrinsic WVTR of 1.41×10^{-4} g/m^2 day at 50 °C/85% RH. Due to the low defect density of the tested barrier film, the defect-assisted WVTR was found to be three times lower than the intrinsic WVTR, and an effective (or total) WVTR value was 1.89×10^{-4} g/m^2 day. Thus, improvements of the barrier performance should focus on reducing the number of defects while also improving the intrinsic barrier performance of the hybrid layer. © *2016 AIP Publishing LLC.* [http://dx.doi.org/10.1063/1.4942510]

INTRODUCTION

The development of barrier film technology to reduce the permeation of oxygen and water vapor is important to provide semi-hermetic packaging for various applications including the food, pharmaceutical, and electronics industries. In particular, with the increasing interest in organic electronic devices, research in the development of ultrabarrier films has become important in order to increase their lifetime.[1–3] The requirement of a barrier film for the organic electronic devices varies depending on the application such as organic light-emitting diodes (OLED), organic photovoltaics (OPV), and organic thin-film transistors (OTFT). In general, the effective water vapor transmission rate (WVTR) of a barrier film is higher than the intrinsic WVTR due to the presence of pinholes and macroscopic defects arising during the manufacturing process.[4–6] However, the measured value of the WVTR does not provide sufficient information to determine if the WVTR for a particular film is governed by the intrinsic value of permeation or by pinholes and other defects. Thus, better knowledge of the different contributions from intrinsic permeation and defect permeation will enable better engineering of advanced ultrabarriers, placing the focus more on defect mitigation during manufacturing while improving the intrinsic quality of the barrier. In general, a device can be packaged with a barrier coating either by direct encapsulation or by indirect encapsulation, as shown in Figure 1.[1] Direct encapsulation is a method where the barrier film is coated directly on top of a device. Indirect encapsulation is a method where a barrier film is separately prepared on an independent substrate and then subsequently sealed over the device. In the latter case, the barrier film is attached using an edge sealant or an adhesive film.

A common approach to measure the WVTR of a barrier film is to replace the device in Figure 1 with a calcium layer which corrodes in the presence of oxygen and water.[7,8] The WVTR of the barrier film can be evaluated from this experiment by estimating the amount of calcium that reacts with water vapor either optically or electrically.[7,9,10] Using a calcium corrosion test with a direct encapsulation barrier, Carcia *et al.* and Meyer *et al.* have reported WVTR values as low as 10^{-5} g/m^2 day.[10,11] However, these WVTR values are estimated with small sized samples (0.25-40 mm^2). In optical tests, the reported WVTR values are estimated either only by evaluating the calcium layer thickness change in the pinhole-free area[12] or by accounting the area changes of a fully degraded portion in the calcium layer.[13] Therefore, neither of the methods can differentiate between the dominant permeation mechanisms in the barrier film (e.g., intrinsic permeation through a barrier or by defect-assisted local permeation). In an alternate configuration, the barrier film is tested with a gas space above the calcium sensor as shown in Figure 1(b). In this case, the measured value is always an effective WVTR. However, the dominant permeation mechanism which contributes to the effective WVTR is not known from such experiments. Roberts *et al.*[6] and Affinito and Hilliard[14] have studied

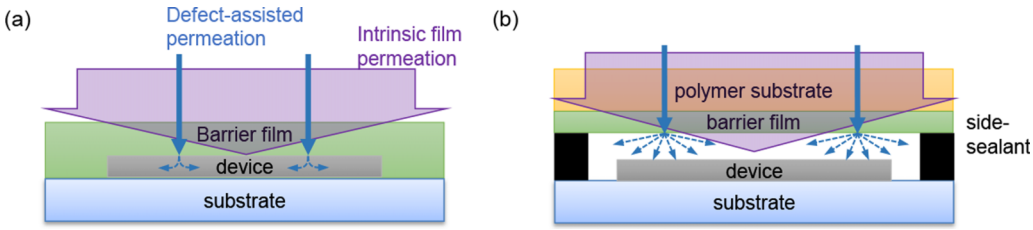

FIG. 1. Two different approaches of barrier film encapsulation: (a) direct encapsulation and (b) indirect encapsulation. Pathways of the intrinsic film permeation and defect-assisted permeation are illustrated with a purple wide arrow and blue narrow arrows, respectively.

theoretically the contribution of pinholes with different sizes for WVTR in an independent barrier film. However, experimental methods to determine the WVTR have not been widely developed and employed.

For defect-assisted permeation through a barrier film (inorganic barrier coating on polymers) applied by indirect encapsulation, Rossi and Nulman described a permeation model via a single pinhole with the assumption that the inorganic barrier coating surrounding the pinhole is impermeable.[15] This model was further advanced by da Silva Sobrinho *et al.*[5] A central assumption of these models is that the concentration of water vapor on the side of the barrier film not exposed to humid air is zero, so the concentration gradient or diffusion driving force is maximum. This assumption is valid when the barrier film is encapsulated with a small cavity as shown Figure 1(b) or in chambers such as the MOCON test.[16] However, if a barrier coating is directly deposited on a device as shown in Figure 1(a), then the concentration under the barrier film is unknown because the permeated water vapor through a pinhole can accumulate in the device layer. Thus, the previous assumptions in calculating the WVTR for this condition must be checked in order to appropriately calculate the permeation rate locally using the calcium corrosion test.

In this study, we introduce a characterization method that allows for the discrimination and quantification of the defect-assisted local permeation rate and the barrier film's intrinsic permeation rate by optically monitoring the degradation of directly encapsulated calcium samples. We demonstrate this method by evaluating the barrier properties of an ALD-PECVD hybrid barrier film applied directly on calcium samples. The hybrid barrier was chosen in this study since it has been shown to provide a low WVTR and allows for the tailoring of mechanical stresses which works to mitigate cracking in the vicinity of particle defects found on devices during direct deposition of barrier films.[17] We first acquire sequential images of directly encapsulated calcium samples as a function of the sample exposure time to a humid atmosphere at 50 °C and 85% RH. Image sequences were digitally processed to derive a model that describes the calcium degradation as a function of both the local and intrinsic WVTR for the barrier film by measuring the permeation through each macroscopic defect as well as the defect free region. This method allows for the discrimination of the individual contribution of each mechanism to the effective WVTR and provides statistically relevant information on the permeation through defects in the barrier.

EXPERIMENTAL

Figure 2 shows the diagram of the calcium test sample used for this study. A 100 nm-thick calcium layer was deposited in the form of 16 square patterns (5.09 mm × 5.09 mm) on a 38 mm × 38 mm glass substrate using a thermal evaporator (EvoVac, Angstrom Engineering). The thickness of calcium layer was controlled using a quartz crystal microbalance *in situ*. After that, a 200 nm polymer layer (CYTOP, AGC Chemicals) was spin-coated on the calcium layer in a glove box. The CYTOP was mixed with the solvent (CT-SOLV180, AGC Chemicals). The spin-coated polymer films were cured at 100 °C for 30 min. The purpose of the polymer layer is not only to provide a short-term barrier layer that prevents calcium degradation during sample transport from the glove box to the deposition system but also to reduce pinholes in the barrier film that can be caused by contaminant particles.[17] Afterwards, the sample was transferred to a PECVD system (Oxford) using a vacuum canister, and 100 nm SiN_x was deposited on top of the

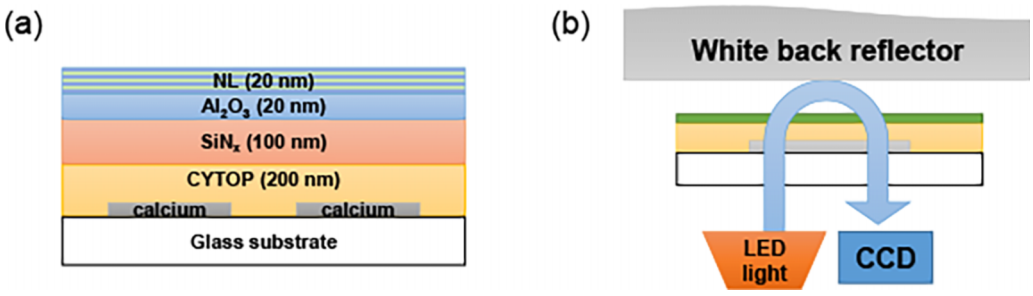

FIG. 2. Schematic diagrams of (a) the calcium degradation test sample encapsulated with a barrier film consisting of SiN_x, Al_2O_3 and Al_2O_3/HfO_x nanolaminate (NL), and (b) the scanning configuration used to capture the image of the Ca sample to determine changes in light transmission through the Ca and regions of localized defects.

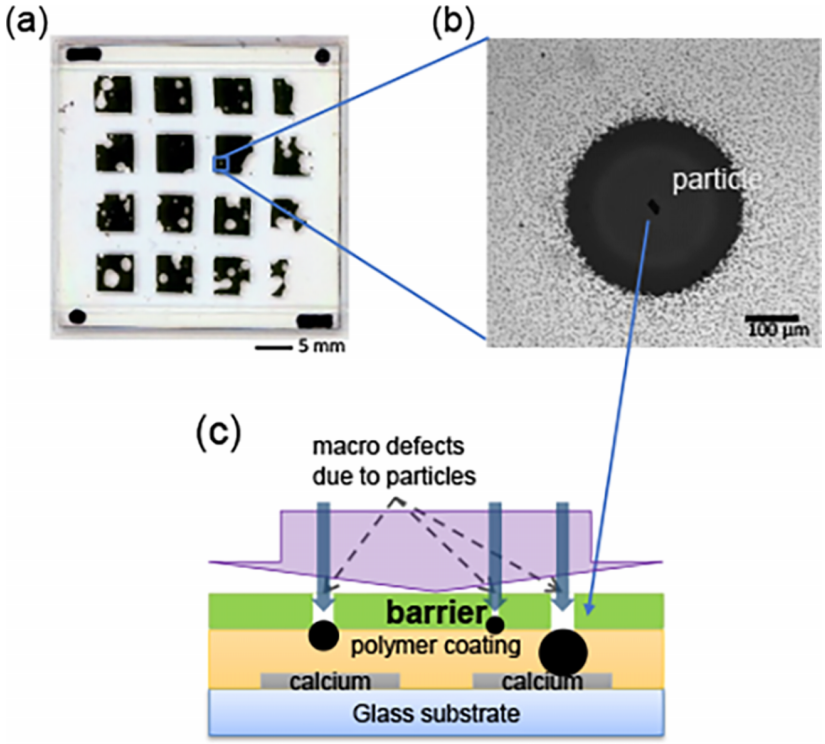

FIG. 3. An example of local degradation of a Ca sensor due to the existence pinholes associated with particle defects. (a) A scanned image of the full 16 calcium square sample after degradation, (b) a zoomed in image of a local degradation spot, and (c) a cross-sectional diagram of devices showing localized high permeation in regions with defects.

CYTOP layer at 100 °C. After the PECVD deposition, a 20 nm Al_2O_3 layer was deposited by atomic layer deposition (ALD) followed by a 20 nm-thick ALD nanolaminate consisting of Al_2O_3 and HfO_x, alternating every 5 cycles. All ALD growth was performed in a Savannah ALD system (Cambridge Nanotech). The details of calcium test sample preparation are described elsewhere.[17]

Directly encapsulated calcium samples were placed in a humidity chamber at 50 °C and 85% RH. Images of the samples were taken periodically in order to track the degradation of the calcium layer using a high-resolution flatbed photo scanner (Epson V600) outside of the humidity chamber. The photo scanner was equipped with a white LED light source along with a charge-coupled device (CCD) image sensor and a white back reflector behind the samples. The color sample images were taken at 2400 dpi resolution in reflection mode as shown in Figure 2(b) without any color correction algorithm. Then, the images were converted into 256-level gray scale images and binary images using MATLAB functions for further analysis to investigate the detail features of the sample degradation. For binary image conversion, an intensity threshold value was determined by Otsu's method using a MATLAB function.[18]

RESULTS AND DISCUSSION

Calcium degradation analysis

First, we observed that the most obvious degradation behavior of the encapsulated calcium layer was correlated with the appearance of macro-sized local degradation spots as shown in Figure 3(a), larger than the pixel size of the 2400 dpi image resolution, 10.6 μm × 10.6 μm. These macro-size local degradation spots were usually accompanied with a particle at the center of the spots. Figure 3(b) shows a microscopic image of one of the local degradation spots, and the associated particle at its center. Thus, it appears to be clear that the local degradation spots arise from pinholes in the barrier film caused by the presence of macroscopic sized particles; much larger than the tens of nanometer-thick layers used in our test samples. Macroscopic particles can lead to the formation of pinholes in the barrier layer because of either residual stress concentration or poor barrier film coverage on the particle (Figure 3(c)).[17] According to the classification of pore sizes by the International Union of Pure and Applied Chemistry (IUPAC),[19,20] the pinhole defects can be classified as macropores (>50 nm) because the observed particle size is on the order of micrometers under a microscope as shown in Figure 3(b). Also, since the radial growth rate of the locally degraded Ca is directly related to the water vapor that is transported through the pinhole defects, analyzing the growth of each of the spots will help to understand the water vapor permeation behavior through the defects.

In addition to the local degradation spots, the images of a calcium sample displayed a change in intensity of the intact calcium area free of the large local defects as in Figure 4(c). The intensity change of the intact area is more visible from intensity histograms of images as in Figure 4(d). This intensity change is due to the uniform degradation of the calcium layer by water vapor permeation through regions of the barrier film that contain only nanoscale size defects or

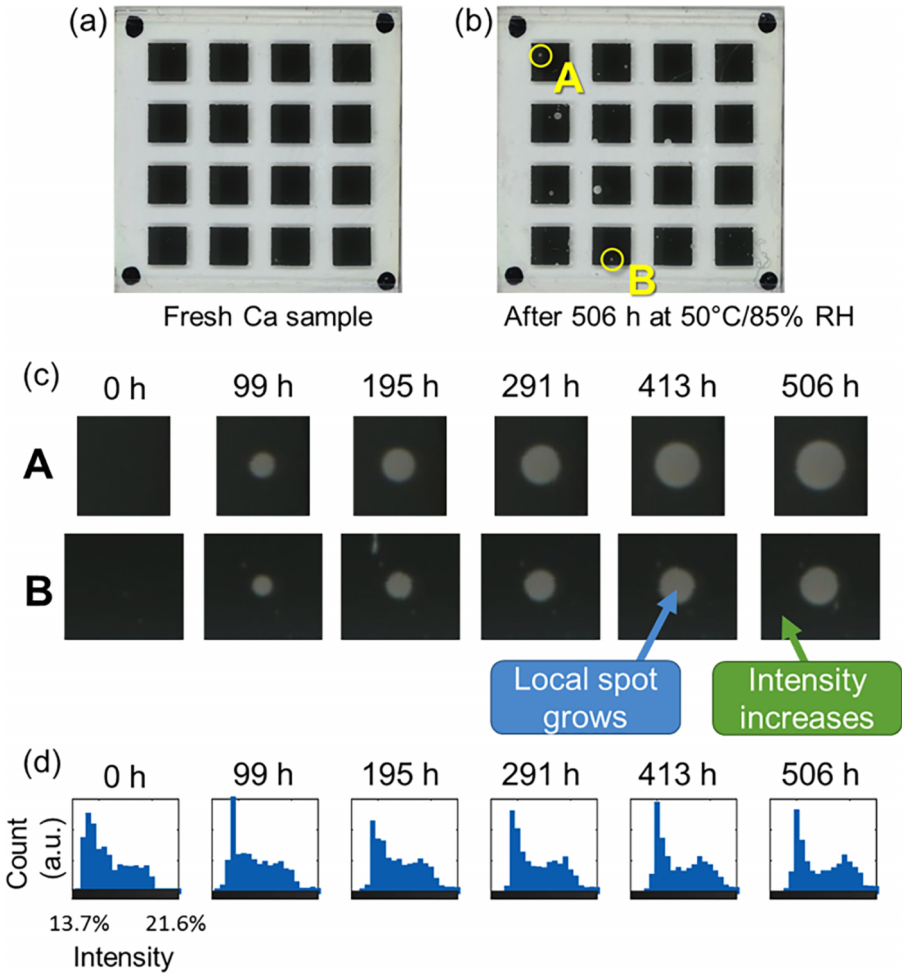

FIG. 4. Calcium sample images of a tested barrier at 50 °C/85% RH. (a) Fresh calcium sample image, (b) an image of the calcium sample after 506 h of degradation, and (c) images showing the growth of selected local degradation spots over time as well as an increase in the intensity through the defect free regions of the Ca sensors. (d) Normalized intensity histogram of spot B images in (c). Only low intensity region is plotted for better discerning changes in intensity or light transmission through the Ca.

porosity that is not detectable by our optical system. In this case, the permeation occurs through uniformly distributed sub-micron defects or porosity in the film. Thus, the reaction of calcium and permeated water vapor flowing through nanoscale porosity is not detectable with the resolution of the image but manifests itself as a change in the intensity of the image. This change is usually reported in the literature as the intrinsic barrier film performance and the permeation through this region is assumed to be negligible in case of barrier films with macroscale defects. Discrimination between the intrinsic permeation rate and the defect-assisted local permeation is critical to better understand the total or effective WVTR of barrier films.

The effective WVTR of the barrier film arises from both the flux through pinholes or defects and the intrinsic flux through the barrier film. In other words, the effective flux of gas permeation in a barrier film can be expressed as

$$J_{eff} = -D_{intrinsic}\frac{\partial C}{\partial x} + J_{pinhole}, \quad (1)$$

where J_{eff} is the effective flux of a barrier film, $D_{intrinsic}$ is the molecular diffusivity of intrinsic film, C is the concentration of gas molecules, and $J_{pinhole}$ is the flux through a pinhole. The evaluation of the defect assisted local WVTR and the intrinsic WVTR can be conducted using the experimental procedure described in this study.

Defect assisted permeation

As described previously, the calcium layer degrades locally due to permeation of water vapor through pinholes or defects in the barrier film, and the degradation appears as a white spot in the sample's image since calcium hydroxide is transparent optically allowing light to reflect from the white background. As seen in Figure 4(c), the calcium hydroxide spot size grows radially over time, suggesting that the permeated water vapor via the pinhole diffuses isotropically inside the layers under the barrier film. Figure 5(a) shows calcium sample images after 506 h at 50 °C/85% RH. From the images, local degradation spots that are independent from each other are selected. Then, the radius and the area of the select spots are measured from the binary images using a feature extraction function of MATLAB and plotted in Figures 5(b) and 5(c), respectively. Differences in pinhole size lead to a large variance in the growth rate between calcium hydroxide spots. However, the temporal evolution of

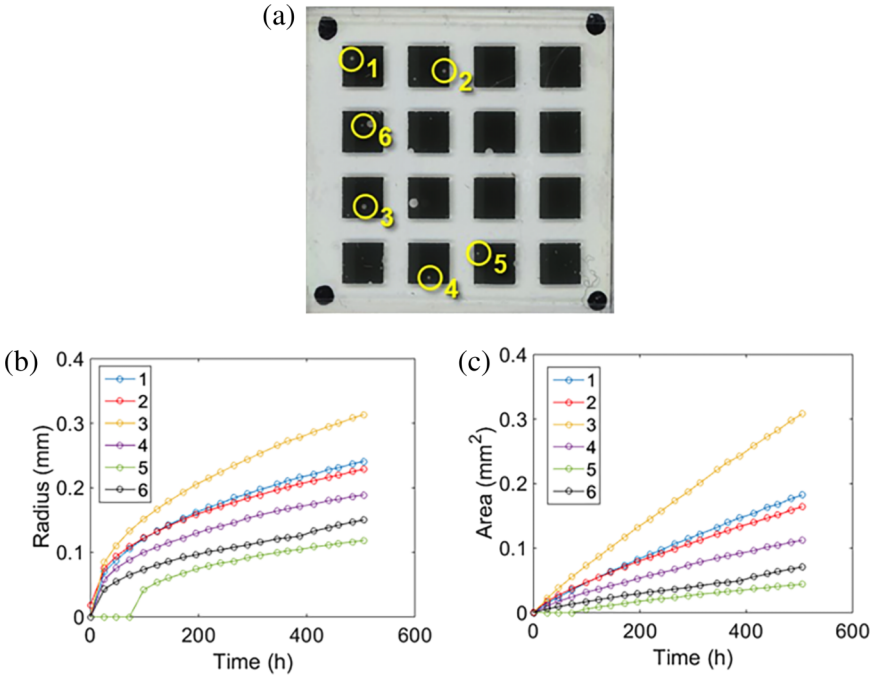

FIG. 5. Growth of local degradation spots over time: (a) Local degradation spots chosen from the 16 Ca sensors, (b) change in the radius of the selected local degradation spots versus time, and (c) change in area of the selected local degradation spots versus time.

the spot radii displays a similar functional dependence over time, while the area of each spot increases approximately linearly over time.

From the experimental results, it is reasonable to consider that the growth of calcium hydroxide spot is due to a radial diffusion process of water vapor inside the underlying layer, modeled through a 1-dimensional radial diffusion equation,

$$\frac{\partial C}{\partial t} = D\nabla^2 C = D\frac{1}{r}\frac{\partial}{\partial r}\left(r\frac{\partial C}{\partial r}\right), \quad (2)$$

where t is time and r is the radial position[21] as shown in Figure 6(a). This model has a semi-infinite boundary condition that $C = 0$ as r goes infinity, but the other boundary condition at $r = 0$ is not clear. If the boundary condition is a constant concentration, $C = C_0$ at $r = 0$, Eq. (2) is solvable using the separation of variable method, and the solution of the Eq. (2) is expressed by Bessel functions,

$$C = \sum_{n=1}^{\infty} \exp(-\lambda_n^2 Dt)\left[C_{1,n}J_0(\lambda_n r) + C_{2,n}Y_0(\lambda_n r)\right], \quad (3)$$

whereas, if the boundary condition is a constant total flux condition, $Q = Q_0$ at $r = r_0$, Eq. (2) is solvable using a similarity function, and the solution is

$$C = C_0 \int_{\eta}^{\infty} \frac{1}{\eta'} \exp\left(-\eta'^2\right) d\eta', \quad (4)$$

where the similarity function, η, is defined as $\eta = r/\sqrt{4Dt}$.

From the solutions for both cases, Figures 6(b) and 6(c) plot the contour profiles of the concentration with r versus t for both boundary condition, respectively. Even if the constants such as D, C_0, Q_0, and r_0 were arbitrarily selected, Figures 6(b) and 6(c) clearly show the difference of the profiles over time because of the different boundary condition. In case of constant concentration condition, the diffusion rate decreases more rapidly than the case of constant flux condition over the time. Between the two conditions, it is apparent that the solution with a constant total flux boundary condition (Figure 6(c)) coincides with the radial growth profiles from the experimental results (Figure 5(b)). Recalling that the spot area corresponds to the amount of water vapor in a calcium test and the growth rate of the spot area is constant, these modeling results suggest that the local degradation follows a radial diffusion process with a constant total flux condition. In other words, the permeation rate through a pinhole is constant over time even if the barrier film is directly deposited on the device.

Intrinsic film permeation

In addition to the defect assisted local degradation, the calcium layer appears to degrade uniformly in absence of local pinhole defects, as seen in Figure 4(c). The uniform calcium degradation appears as a transparency change of the intact calcium layer. If we assume that the calcium oxidation progresses uniformly, forming a calcium hydroxide layer on the top of the calcium layer, the remaining calcium thickness can be determined from the transparency of the calcium layer.

The transparency of the calcium layer in a pinhole-free area is evaluated through the following procedure. From an original image (Figure 7(a)), the pinhole-free area is selected from an intensity threshold value determined by Otsu's method.[18] Figure 7(b) plots the histogram of the original image with the threshold value (red vertical line), and Figure 7(c) shows the selected intact calcium area as white color in a binary image. Referring the binary

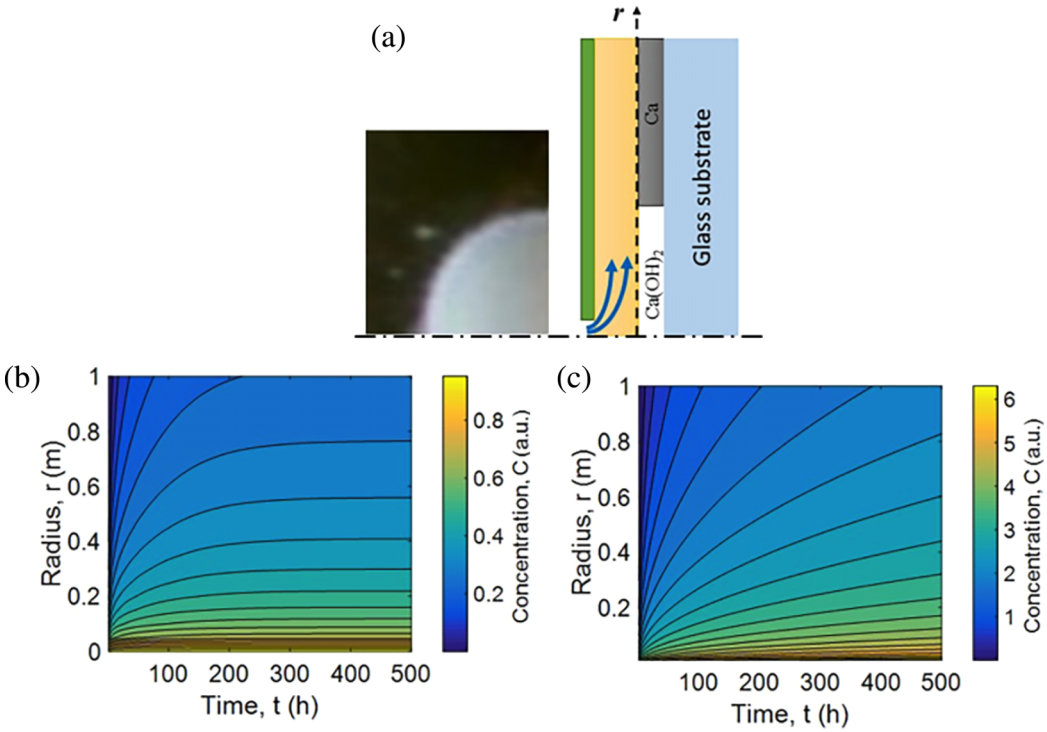

FIG. 6. A depiction of the 1D radial diffusion model of water vapor permeation inside the underlying layers of the barrier film. (a) A diffusion model diagram with a quarter symmetry image of a local degradation spot, (b) the concentration contour plot on radius vs. time plane with a constant concentration boundary condition at the center ($C = C_0$ at $r = 0$), and (c) the concentration profile on radius vs. time plane with a constant total flux boundary condition, $Q = Q_0$ at $r = r_0$.

image, the original intensity of the pixels that are within the selected defect-free area is averaged. Afterwards, the transparency and the thickness of the remaining calcium layer are determined from the average pixel intensity by neglecting interference effects and using Beer-Lambert law,

$$\frac{I_{Ca\_area}}{I_{background}} \approx \frac{I_{source}(T_{substrate}T_{Ca}T_{barrier})^2 R_{back}}{I_{source}(T_{substrate}T_{barrier})^2 R_{back}} = {T_{Ca}}^2 = \exp(-\alpha_{Ca}h_{Ca})^2, \quad (5)$$

where I_{Ca_area} *and* $I_{background}$ are the average intensity of select calcium area and background area, respectively. I_{source} is the intensity of the light source. T is the transparency of each layer, R_{back} is the reflectance of the white back reflector, and α_{Ca} and h_{Ca} are the attenuation coefficient and the thickness of a calcium layer, respectively. Since α_{Ca} is a function of wavelength, it is difficult to calculate the representative value without knowing the spectrum of the incident light on the calcium layer. Instead, an effective α_{Ca} is estimated using the calcium transparency of the first image ($t = 0$) with the assumption that the thickness of calcium layer is 100 nm as deposited. Finally, Figure 7(d) plots the average pixel intensity and the estimated calcium thickness versus time. The calcium thickness decreases linearly up to 500 h in this barrier film test at 50 °C/85% RH.

Overall permeation

The WVTR of the barrier film is estimated from the amount of calcium degradation that was analyzed previously for the two permeation pathways; defect assisted local degradation and intrinsic permeation. If we assume that the permeated water vapor has reacted with calcium, the WVTR for each permeation pathway through the barrier film can be estimated from the degree of calcium degradation. For a defect assisted local permeation, the amount of water vapor that permeates through the barrier is proportional to the mass of calcium layer that reacts with water, which is measurable from the area of local degradation spot in the scanned image. Therefore, the water vapor transport rate for a single spot is

$$Q_{defect} = 2\frac{M_{water}}{M_{Ca}}\rho_{Ca}h_{Ca}\frac{\partial A_{spot}}{\partial t}, \quad (6)$$

where M_{water} and M_{Ca} are the molecular weight of water (18.02 g/mol) and calcium (40.1 g/mol), respectively, ρ_{Ca} and h_{Ca} are the density (1.55 g/cm^3) and the thickness of the calcium layer (100 nm), respectively. Thus, WVTR of all spots per area is the summation of all local degradation spots

$$WVTR_{defect} = \frac{1}{A_{barrier,0}}\sum_i^N Q_{defect,i} = 2\frac{1}{A_{barrier,0}}\frac{M_{water}}{M_{Ca}} \times \rho_{Ca}h_{Ca}\sum_i^N \frac{\partial A_{spot,i}}{\partial t}, \quad (7)$$

where $A_{barrier,0}$ is the area of the barrier film (415 mm^2), and N is the number of spots. The total area growth rate of all the spots in the sample is calculated by finding the total spot area changes from whole binary images instead of accounting individual defect spots and is found to be 0.145 mm^2/day. The average and the standard deviation of the spot area growth rate in 16 calcium squares are shown to be 9.1×10^{-3} mm^2/day and

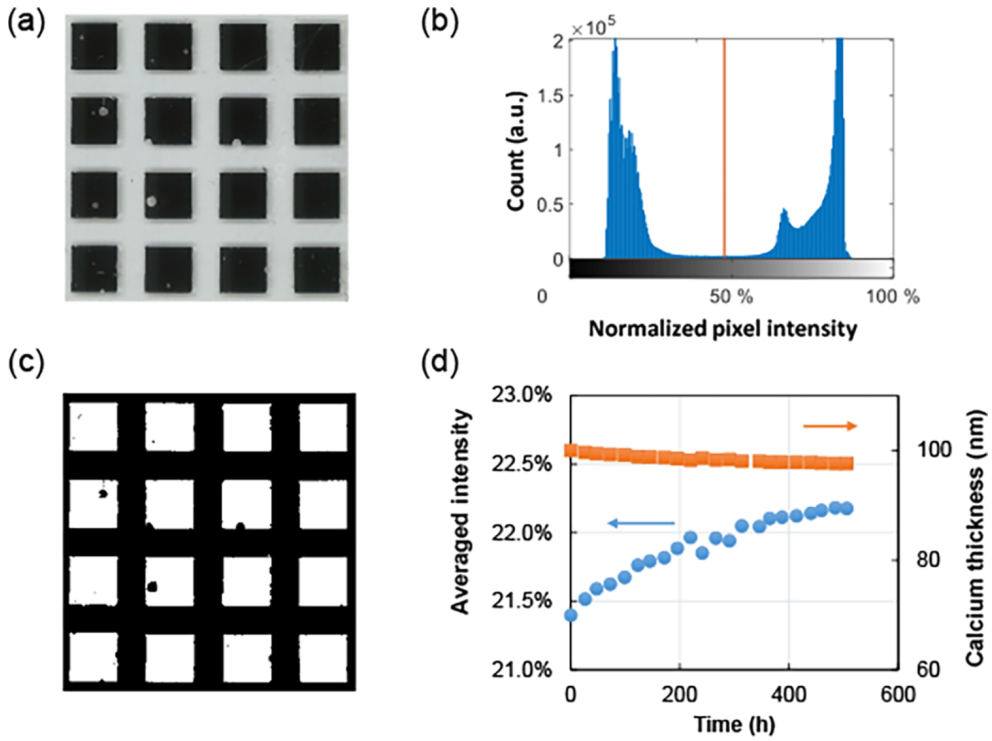

FIG. 7. Uniform degradation of the calcium layer and the evaluation of the degradation. (a) An original sample image after 506 h, (b) histogram of the original image with a threshold value shown by the orange vertical line, (c) binary image of the intact calcium region, selected using the threshold value, and (d) average intensity change and thickness change of the intact calcium area over time.

1.53×10^{-2} mm^2/day, respectively. Since defects are distributed randomly on several calcium squares in the sample, the standard deviation is relatively large. The total area growth rate results in the $WVTR_{defect}$ as 4.84×10^{-5} g/m^2 day using Eq. (7).

The intrinsic WVTR of the barrier film is proportional to the rate of thickness decrease of the calcium layer and is expressed as

$$WVTR_{intrinsic} = 2\frac{M_{water}}{M_{Ca}}\rho_{Ca}A_{Ca}\frac{\partial h_{Ca}}{\partial t}\frac{1}{A_{barrier}}, \quad (8)$$

where A_{Ca} and $A_{barrier}$ are equal when a barrier film is directly deposited on the Ca layer. The rate of thickness decrease of the tested calcium samples was found to be −0.102 nm/day using the slope of Figure 7(d), and the $WVTR_{intrinsic}$ was calculated to be 1.41×10^{-4} g/m^2 day using Eq. (8).

Finally, the effective WVTR of a barrier film is the summation of the two WVTR values, Eqs. (7) and (8),

$$WVTR_{eff} = WVTR_{defect} + WVTR_{intrinsic}. \quad (9)$$

Using Eq. (9) and the previous results of the calcium degradation analysis, the effective WVTR of the tested barrier film was calculated as 1.89×10^{-4} g/m^2 day at 50 °C/85% RH. As a result, the intrinsic permeation rate contributes ca. 3 times more to the effective WVTR than the defect assisted local permeation rate in the tested barrier film. However, since the defect assisted WVTR is dependent on the defect density in a given barrier film, the ratio is also dependent on the conditions of barrier film fabrication process, such as handling and cleanliness of the environment. For example, an inferior barrier film (Figure 3(a)) that was prepared in uncontrolled environments shows much higher defect density than the tested barrier film (Figure 4(b)), and the contribution of the defect assisted WVTR is more dominant than the intrinsic film permeation in the inferior barrier film.

CONCLUSION

By studying the contributions to WVTR from the intrinsic and defect driven permeation pathways, a better understanding of the effective WVTR of a barrier film can be obtained. By employing optical calcium corrosion test, it is possible to observe the results of these two permeation mechanisms independently. The defect-assisted WVTR was estimated from the area growth rate of local calcium degradation spots, and the continuous layer intrinsic barrier film WVTR was evaluated from the transparency change rate of the intact calcium area. Comparing the area growth rate of the local degradation spot with a cylindrical diffusion model, it was found that the WVTR though a pinhole is constant with a negligible lag time. Since the defect-assisted WVTR is dependent on the size of the pinholes and the number density of pinholes in a barrier film, they can contribute a significant amount to the overall permeation, if they are not controlled during the fabrication process. For low defect densities, as shown in this study, the WVTR is dominated by the intrinsic permeation through the barrier film. Thus, efforts to reduce the WVTR should focus on improving the intrinsic properties of the barrier. In addition, local defects should be reduced in order to prevent local degradation of devices in the vicinity of defects. However, other methods such as multilayer films or the use of getters may help address these issues.

ACKNOWLEDGMENTS

This material is based upon work supported by the Department of Energy through the Bay Area Photovoltaic Consortium under Award No. DE-EE0004946.

[1]J. S. Lewis and M. S. Weaver, IEEE J. Sel. Top. Quantum Electron. **10**, 45 (2004).
[2]J. Ahmad, K. Bazaka, L. J. Anderson, R. D. White, and M. V. Jacob, Renewable Sustainable Energy Rev. **27**, 104 (2013).
[3]G. J. Jorgensen, K. M. Terwilliger, J. A. DelCueto, S. H. Glick, M. D. Kempe, J. W. Pankow, F. J. Pern, and T. J. McMahon, Sol. Energy Mater. Sol. Cells **90**, 2739 (2006).
[4]A. S. da Silva Sobrinho, G. Czeremuszkin, M. Latrèche, G. Dennler, and M. R. Wertheimer, Surf. Coat. Technol. **116–119**, 1204 (1999).
[5]A. S. da Silva sobrinho, G. Czeremuszkin, M. Latrèche, and M. R. Wertheimer, J. Vac. Sci. Technol., A **18**, 149 (2000).
[6]A. P. Roberts, B. M. Henry, A. P. Sutton, C. R. M. Grovenor, G. A. D. Briggs, T. Miyamoto, A. Kano, Y. Tsukahara, and M. Yanaka, J. Membr. Sci. **208**, 75 (2002).
[7]G. Nisato, P. C. P. Bouten, P. J. Slikkerveer, W. Bennett, G. Graff, N. Rutherford, and L. Wiese, in *Proceedings of Asia Display/IDW'01* (Society for Information Display, 2001), p. 1435.
[8]J. Bertrand, D. Higgs, M. Young, and S. George, J. Phys. Chem. A **117**, 12026 (2013).
[9]M. O. Reese, A. A. Dameron, and M. D. Kempe, Rev. Sci. Instrum. **82**, 085101 (2011).
[10]P. F. Carcia, R. S. McLean, M. D. Groner, A. A. Dameron, and S. M. George, J. Appl. Phys. **106**, 023533 (2009).
[11]J. Meyer, P. Görrn, F. Bertram, S. Hamwi, T. Winkler, H.-H. Johannes, T. Weimann, P. Hinze, T. Riedl, and W. Kowalsky, Adv. Mater. **21**, 1845 (2009).
[12]G. Nisato, H. Klumbies, J. Fahlteich, L. Müller-Meskamp, P. van de Weijer, P. Bouten, C. Boeffel, D. Leunberger, W. Graehlert, S. Edge, S. Cros, P. Brewer, E. Kucukpinar, J. de Girolamo, and P. Srinivasan, Org. Electron. **15**, 3746 (2014).
[13]B. J. Kim, D. H. Kim, S. Y. Kang, S. D. Ahn, and S. G. Im, J. Appl. Polym. Sci. **131**, 40974 (2014).
[14]J. Affinito and D. Hilliard, in *Proceedings of Society of Vacuum Coaters 47th Annual Technical Conference Proceedings* (Society of Vacuum Coaters, 2004), p. 563.
[15]G. Rossi and M. Nulman, J. Appl. Phys. **74**, 5471 (1993).
[16]MOCON, Inc., Instruments: Permeation and Barrier Measurement, http://www.mocon.com/permeation.php; accessed 2015.
[17]A. Bulusu, A. Singh, C. Y. Wang, A. Dindar, C. Fuentes-Hernandez, H. Kim, D. Cullen, B. Kippelen, and S. Graham, J. Appl. Phys. **118**, 085501 (2015).
[18]N. Otsu, IEEE Trans. Syst Man Cybern. **9**, 62 (1979).
[19]A. D. McNaught and A. Wilkinson, *Compendium of Chemical Terminology* (Blackwell Science, Oxford, 1997).
[20]P. Klobes, K. Meyer, and R. G. Munro, *National Institute of Standards and Technology, Porosity and Specific Surface Area Measurements for Solid Materials* (U.S. Department of Commerce, Technology Administration, National Institute of Standards and Technology, 2006).
[21]J. Crank, *The Mathematics of Diffusion* (Oxford University Press, Oxford, 1979).